

Syngas Production via CO₂ Reforming of Methane over Aluminum-Promoted NiO–10Al₂O₃–ZrO₂ Catalyst

Ye Wang, Yannan Wang, Li Li, Chaojun Cui, Xudong Liu, Patrick Da. Costa,* and Changwei Hu*

Cite This: *ACS Omega* 2021, 6, 22383–22394

Read Online

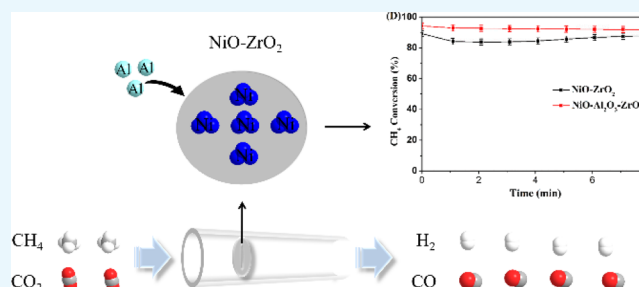
ACCESS |

Metrics & More

Article Recommendations

ABSTRACT: CO₂ reforming of methane was studied at medium temperature (700 °C) using a GSHV of 48,000 h⁻¹ over nickel catalysts supported on ZrO₂ promoted by alumina. The catalysts were prepared by a one-step synthesis method and characterized by BET, H₂-TPR, XRD, XPS, TEM, Raman spectroscopy, and TGA. The NiO–10Al₂O₃–ZrO₂ catalyst exhibited higher catalytic performance in comparison with the NiO–ZrO₂ catalyst. The enhancement of catalytic activity in dry reforming could be associated with the alterations in surface properties due to Al promotion. First, the Al promoter could modify the structure of ZrO₂, leading to an increase of its pore volume and pore diameter.

Second, the NiO–10Al₂O₃–ZrO₂ catalyst exhibited high resistance to sintering. Third, the NiO–10Al₂O₃–ZrO₂ catalyst showed high suppression to the loss of nickel during a long-term catalytic test. Finally, the addition of Al could inhibit the reduction of ZrO₂ during the reduction and reaction, endowing further the stability.



INTRODUCTION

In recent years, the reaction of carbon dioxide reforming of methane, which is defined as the dry reforming of methane (DRM), has garnered extensive attention among scientific researchers. It utilizes two greenhouse gases (CO₂ and CH₄) to produce syngas (CO and H₂), which can be further converted to methanol or fuels through Fisher–Tropsch synthesis.^{1–3} Therefore, the global warming issues could be mitigated through the deep investigation of the DRM reaction.

According to the literature, a large number of parallel side reactions, such as the CO disproportionation, CH₄ decomposition, reverse water gas shift, and so on (Table 1), might take place during the DRM reaction.^{4–6} The reverse water gas shift reaction would consume H₂ and reduce the H₂/CO molar ratio.

Table 1. Possible Parallel Reactions during the Dry Reforming of Methane

reaction number	reaction	ΔH°_{298K} KJ/mol
1	dry reforming	+247
	$\text{CO}_2 + \text{CH}_4 \rightarrow \text{CO} + \text{H}_2$	
2	reverse water gas shift	+41
	$\text{CO}_2 + \text{H}_2 \rightarrow 2\text{CO} + \text{H}_2\text{O}$	
3	carbon-forming reactions	+74.9
	$\text{CH}_4 \rightarrow \text{C} + 2\text{H}_2$	
	$2\text{CO} \rightarrow \text{C} + \text{CO}_2$	
	$\text{CO} + \text{H}_2 \rightarrow \text{C} + \text{H}_2\text{O}$	
4	$\text{CO} + \text{H}_2 \rightarrow \text{C} + \text{H}_2\text{O}$	-172.4
5	$\text{CO} + \text{H}_2 \rightarrow \text{C} + \text{H}_2\text{O}$	-131.3
6	$\text{CO}_2 + 2\text{H}_2 \rightarrow \text{C} + 2\text{H}_2\text{O}$	-90

The CO disproportionation and CH₄ decomposition led to carbon deposition.

Nickel shows excellent catalytic activity as noble ones (Pt, Ru, and Rh), and Ni-based catalysts have been widely reported for the DRM reaction.^{7–10} Pompeo et al.⁹ compared the catalytic performance of Ni and Pt supported on α -Al₂O₃, ZrO₂ and α -Al₂O₃–ZrO₂ catalysts for the dry reforming of methane. They found that nickel was slightly more active than platinum. Moreover, the nickel-based catalysts served as the optimal alternatives considering economic viability.¹¹ However, the deactivation of Ni-based catalysts due to sintering and/or carbon deposit needs to be addressed in order to achieve facile scaling-up in the industrial process. Thus, tremendous efforts have been focused on the development of promoters or novel support materials to address these two problems, further contributing to the design of catalysts with higher stability.^{12,13}

It has been found that aluminum (Al) as a promoter and/or support could enhance the catalytic performance mainly because Al could improve the reducibility and dispersion of nickel. Liu et al.¹⁴ investigated the effect of La, Al, and Mn promoters on Fe-modified natural clay-supported Ni catalysts for the dry

Received: June 17, 2021

Accepted: August 9, 2021

Published: August 18, 2021



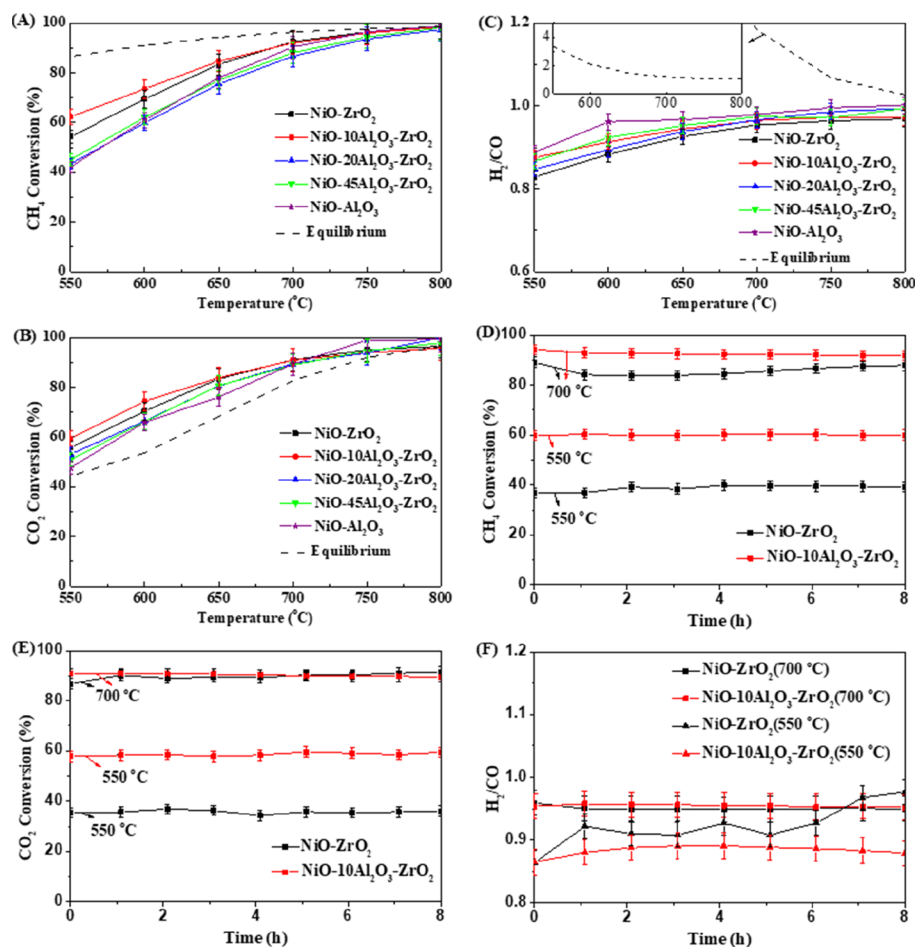


Figure 1. (A) CH_4 conversion as function of temperature, (B) CO_2 conversion as function of temperature, and (C) H_2/CO ratio as function of temperature; $\text{CH}_4:\text{CO}_2:\text{Ar} = 10:10:80$, $\text{GSHV} = 48,000 \text{ h}^{-1}$. CH_4 conversion (D), CO_2 conversion (E), and the H_2/CO ratio (F) in isothermal conditions ($700 \text{ }^\circ\text{C}$ and $550 \text{ }^\circ\text{C}$) on $\text{NiO}-10\text{Al}_2\text{O}_3-\text{ZrO}_2$ and $\text{NiO}-\text{ZrO}_2$ catalysts in the presence of $\text{CH}_4:\text{CO}_2:\text{Ar} = 10:10:80$; $\text{GSHV} = 48,000 \text{ h}^{-1}$.

reforming of methane, and confirmed that the Al-promoted catalyst exhibited the highest catalytic performance in the dry reforming of methane since Al could improve the dispersion and reducibility of nickel species. Talkhonchek and Haghghi¹⁵ found that $\text{Ni}/\text{Al}_2\text{O}_3$ nanocatalysts exhibited the best performance among $\text{Ni}/\text{clinoptilolite}$ and Ni/CeO_2 due to the higher specific surface area, homogenous distributions, and good dispersion of Ni species. Various supports have been employed, such as CeO_2 , ZrO_2 , SiO_2 , La_2O_3 , and Al_2O_3 .^{16–18} ZrO_2 exhibits favorable properties such as thermal stability, oxygen storage capacity, enhancement of the metallic dispersion, and the ability of CO_2 adsorption.^{19–21} Therefore, many researchers have focused on the utilization of ZrO_2 support for DRM. Pompeo et al.⁹ found that ZrO_2 as a basic support could promote the adsorption of CO_2 , thereby inhibiting the carbon deposition. Mesoporous $\text{La}_2\text{O}_3-\text{ZrO}_2$ could promote the stability of the catalyst due to the high dispersion of nickel species.²² Miao et al.²³ found that mesoporous-ZrAl-10 (M-ZrAl-10) with the Al content of 10% exhibited better physical properties than the mesoporous- ZrO_2 (M- ZrO_2) support. The specific surface area increased from 9.8 to $56 \text{ m}^2/\text{g}$, the pore volume increased from 0.07 to $0.13 \text{ cm}^3/\text{g}$, and the pore size distribution decreased from 23.9 to 8.2 nm by the addition of 10 wt % Al. On one hand, the properties of ZrO_2 support could be modified by the introduction of alumina species. On the other hand, ZrO_2 could enhance the performance of the catalyst with Al_2O_3 support for

the dry reforming of methane. Therdthianwong et al.^{24,25} demonstrated that the $\text{Ni}/\text{Al}_2\text{O}_3$ catalyst modified by ZrO_2 exhibited higher stability for the dry reforming of methane because ZrO_2 could promote the elimination of carbon deposition by the dissociation of CO_2 to form oxygen intermediates. The spinel NiAl_2O_4 that formed under the reduction process at higher temperature results in lower activity. The zirconia addition could avoid the formation of spinel NiAl_2O_4 .²⁶ Li and Wang²⁷ also found that the interaction between nickel and the $\text{Al}_2\text{O}_3-\text{ZrO}_2$ support could avoid the formation of spinel NiAl_2O_4 .

Thus, to combine the advantages of Al and Zr, a series of $10\text{NiO}-x\text{Al}_2\text{O}_3-(90-x)\text{ZrO}_2$ ($x = 0, 10, 20, 45, 90$) catalysts were prepared by a one-step synthesis method and tested in the dry reforming of methane. A correlation between the structure and reactivity of promoted and non-promoted catalysts was proposed here in order to highlight the positive effects of aluminum promotion on the catalytic activity in the DRM reaction.

RESULTS AND DISCUSSION

Catalytic Performance in the Dry Reforming of Methane. The catalytic results of the DRM in terms of CO_2 and CH_4 conversion and the ratio of H_2/CO with the range of $550-800 \text{ }^\circ\text{C}$ are presented in Figure 1. Within the series of $10\text{NiO}-x\text{Al}_2\text{O}_3-(90-x)\text{ZrO}_2$ catalysts, $\text{NiO}-10\text{Al}_2\text{O}_3-\text{ZrO}_2$

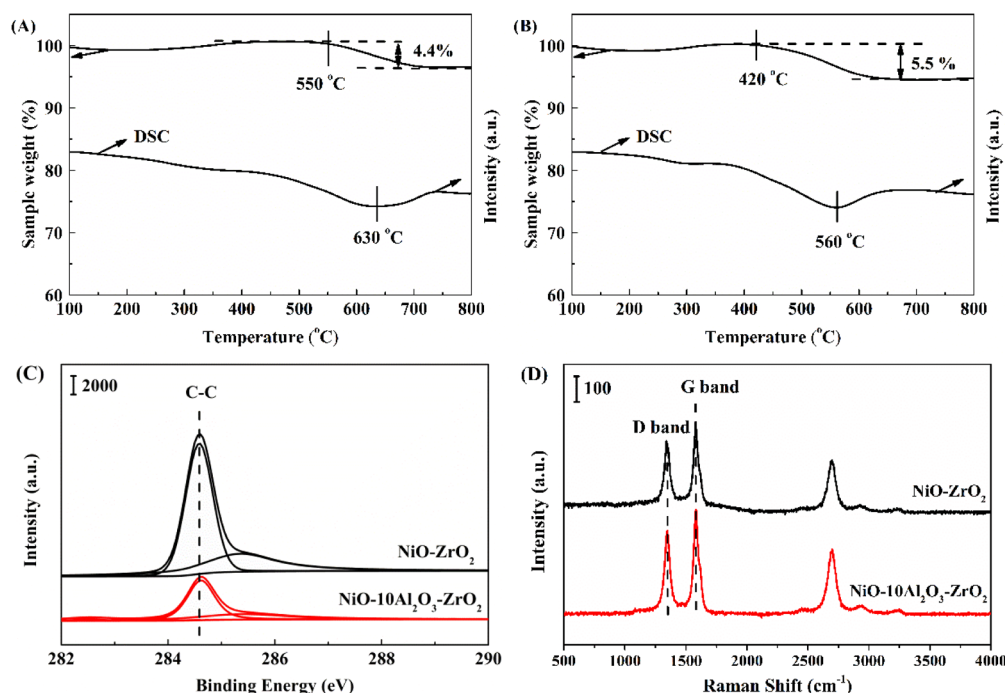


Figure 2. TGA profiles of (A) NiO-ZrO₂ and (B) NiO-10Al₂O₃-ZrO₂ catalysts after reaction at 700 °C for 8 h. (C) C 1s profiles from XPS spectroscopy and (D) Raman profiles of NiO-ZrO₂ and NiO-10Al₂O₃-ZrO₂ catalysts after reaction at 700 °C for 8 h.

exhibited the highest CH₄ conversion in the whole temperature range during the DRM experiment. This advantage became more prevalent with the decrease of reaction temperature, especially at 550 °C. On all the catalysts, the obtained CH₄ conversion was always lower than the equilibrium conversions of CH₄. From Figure 1A, the conversion of methane at 550 °C obtained for NiO-ZrO₂, NiO-10Al₂O₃-ZrO₂, NiO-20Al₂O₃-ZrO₂, NiO-45Al₂O₃-ZrO₂, and NiO-Al₂O₃ catalysts were 54, 62, 43, 45, and 42%, respectively. A similar trend was observed in CO₂ conversion with the following results obtained at 550 °C: 56, 59, 53, 50, and 48% for NiO-ZrO₂, NiO-10Al₂O₃-ZrO₂, NiO-20Al₂O₃-ZrO₂, NiO-45Al₂O₃-ZrO₂, and NiO-Al₂O₃ catalysts, respectively (Figure 1B). The CO₂ conversion of all studied catalysts was also found higher than the equilibrium conversions of CO₂. Meanwhile, the conversion of CO₂ on the NiO-ZrO₂ catalyst was higher than CH₄ conversion, which indicated that the reverse water gas shift reaction (RWGS) occurred. The RWGS reaction would lead to lower the H₂/CO ratio; therefore, the H₂/CO ratio on catalysts was lower than the unity H₂/CO ratio (Figure 1C). In addition, the H₂/CO ratio increased by adding aluminum, indicating that the aluminum could enhance the selectivity to H₂ of the catalyst. Similar results on the effect of Al have also been reported by Liu et al.¹⁴ and Chai et al.²⁸

The stability runs were performed on NiO-10Al₂O₃-ZrO₂ and NiO-ZrO₂ catalysts at 700 °C, and the results are presented in Figure 1. At 550 °C, the conversions of CH₄ and CO₂ on the NiO-10Al₂O₃-ZrO₂ catalyst were higher than those on the NiO-ZrO₂ catalyst, while the H₂/CO ratio on the NiO-10Al₂O₃-ZrO₂ catalyst was lower than the one on the NiO-ZrO₂ catalyst with time on stream. Both catalysts exhibited stable catalytic performance for the DRM reaction. At 700 °C, for the methane conversion, a decrease was observed from 89 to 84% on the NiO-ZrO₂ catalyst within 1 h. The NiO-10Al₂O₃-ZrO₂ catalyst exhibited higher methane conversion, and its conversion remained almost constant at ca. 92%. For the CO₂

conversion, an increase was observed with time on stream on the NiO-ZrO₂ catalyst, which was slightly higher than the one on the NiO-10Al₂O₃-ZrO₂ catalyst after an 8 h run. Meanwhile, the H₂/CO ratio on the NiO-ZrO₂ catalyst was slightly lower than the one on the NiO-10Al₂O₃-ZrO₂ catalyst.

Carbon Formation on NiO-ZrO₂ and NiO-10Al₂O₃-ZrO₂ Catalysts. The carbon deposition of both catalysts was followed by TGA experiments and is shown in Figure 2. The carbon formation on the NiO-10Al₂O₃-ZrO₂ catalyst (5.5%) (Figure 2B) was slightly higher than that found for the NiO-ZrO₂ catalyst (4.4%) (Figure 2A), which can be ascribed to a slight decrease in CO₂ conversion on the NiO-10Al₂O₃-ZrO₂ catalyst during 8 h on-stream. In addition, an increase peak in the sample weight curve could be observed on both NiO-ZrO₂ and NiO-10Al₂O₃-ZrO₂ catalysts due to the oxidation of the Ni⁰ species, implying that there was nickel metal on both catalysts after reaction.^{29,30} The mass value increased over 100% on the NiO-ZrO₂ catalyst since the increasing value obtained by the oxidation of the Ni⁰ species was higher than the decreasing value obtained by the elimination of carbon deposition, and similar results have been reported.²⁹ More carbon that can be removed at 420 °C formed on NiO-10Al₂O₃-ZrO₂ catalysts after reaction, resulting in the mass value not over 100%. From the DSC curve, one peak corresponding to the maximum of carbon consumption at ca. 560 °C for the NiO-10Al₂O₃-ZrO₂ catalyst was observed, whereas a shift to higher temperature (630 °C) was observed for the NiO-ZrO₂ catalyst. It is worth noting that the initial carbon removal temperatures (the initial decrease of sample weight) on NiO-ZrO₂ and NiO-10Al₂O₃-ZrO₂ catalysts are 550 and 420 °C, named as C1 and C2, respectively. Thus, the formed carbon was easier to be removed on NiO-10Al₂O₃-ZrO₂ catalysts, which contributes to the stability of the catalyst. In order to distinguish the types of formed carbon, XPS and Raman spectroscopy experiments were conducted (Figure 2C,D). From the C 1s extracted from XPS data, the peak at about 284.6 eV is attributed to the C-C species and the

adsorbed oil pump molecules (C–C and C–H species). Another peak at 285.5 eV was assigned to the C–O and C=O species.^{31,32} The proportions of the surface C–C, C–O, and C=O species are listed in Table 2. The proportions of C–C and C–H species on NiO–ZrO₂ and NiO–10Al₂O₃–ZrO₂ catalysts were 66 and 63%, respectively.

Table 2. Results of the TGA, XPS, and Raman Experiment for NiO–ZrO₂ and NiO–Al₂O₃–ZrO₂ Catalysts after Reaction at 700 °C for 8 h

catalyst	carbon ^a		C–X species ^b		<i>I_D</i> / <i>I_G</i> ^c
	position/°C	content/%	C–H + C–C	C–O + C=O	
NiO–ZrO ₂	630	4.4	66	34	0.6
NiO–10Al ₂ O ₃ –ZrO ₂	560	5.5	63	37	0.8

^aThe carbon was determined by the TGA method. ^bThe C–X (X = H, O or C) species was determined by XPS. ^cThe *I_D*/*I_G* was determined by Raman spectroscopy.

From the Raman experiment, three distinct peaks (1345, 1580, and 2694 cm^{−1}) could be observed for both NiO–ZrO₂ and NiO–10Al₂O₃–ZrO₂ catalysts. The peaks at about 1345 and 1580 cm^{−1} were assigned to D (disorder) and G (graphite) bands of carbon materials, respectively. The peak at about 2694 cm^{−1} was ascribed to the overtone of the D band (2 × 1345 cm^{−1}

= 2690 cm^{−1}).^{33,34} The intensity of D and G bands are named as *I_D* and *I_G*, respectively. The ratio of *I_D*/*I_G* on NiO–ZrO₂ and NiO–10Al₂O₃–ZrO₂ catalysts are 0.6 and 0.8 (Table 2), respectively. Namely, the type of carbon deposition was mainly in the form of graphite on both catalysts and more graphite formed on the NiO–ZrO₂ catalyst. Combined with XPS and Raman results, the graphite consisted of C–C species, while disorder carbon materials were composed of C–O and C=O species. Those phenomena indicated that the carbon deposition on both NiO–ZrO₂ and NiO–10Al₂O₃–ZrO₂ catalysts was presented as containing graphitic carbon (C–C species). The graphite carbon is generally very difficult to be removed, and the amorphous carbon is easy to be removed.^{35,36} Combined to the results of TGA, XPS, and Raman spectroscopy, the higher content of carbon that is easy to be removed formed on the NiO–10Al₂O₃–ZrO₂ catalyst.

The morphology of carbon deposition on NiO–ZrO₂ and NiO–10Al₂O₃–ZrO₂ catalysts was determined by using transmission electron microscopy. The results are presented in Figure 3. A large amount of carbon in the form of a nanotube were deposited on the NiO–ZrO₂ catalyst (Figure 3A,C), while only some amorphous carbon could be observed on the NiO–10Al₂O₃–ZrO₂ catalyst (Figure 3B,D), which was consistent with the results of XPS and Raman. In addition, the amount of carbon deposition on the NiO–ZrO₂ catalyst (4.4%) was lower than the one on the NiO–10Al₂O₃–ZrO₂ catalyst (5.5%), while the intensity of the C 1s curve in XPS spectra on the NiO–ZrO₂

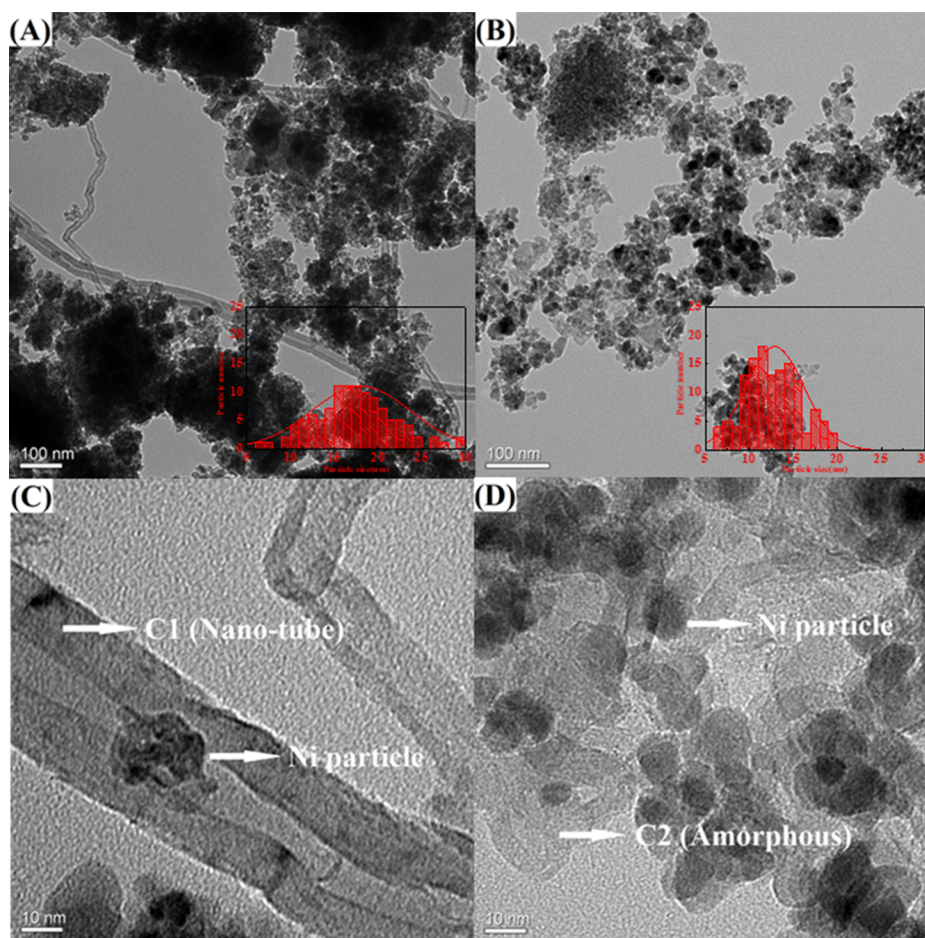


Figure 3. Morphology of (A, C) NiO–ZrO₂ and (B, D) NiO–10Al₂O₃–ZrO₂ catalysts after reaction at 700 °C for 8 h, determined by TEM.

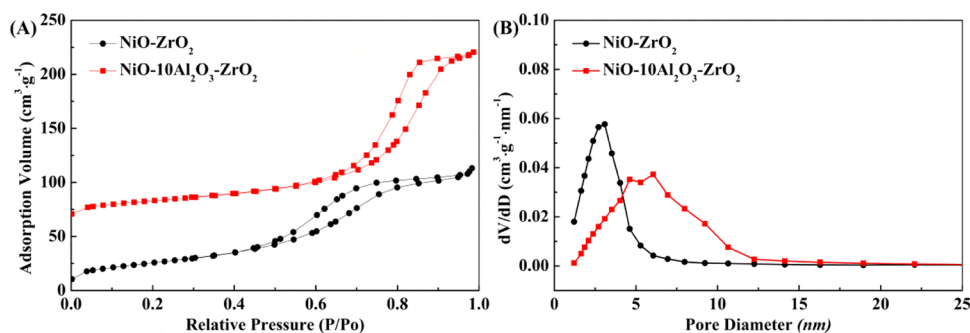


Figure 4. Isotherm (A) and pore size distribution (B) of NiO–ZrO₂ and NiO–Al₂O₃–ZrO₂ catalysts.

Table 3. Results of the BET, XRD, and TEM Experiment for NiO–ZrO₂ and NiO–Al₂O₃–ZrO₂ Catalysts after Reduction and after Reaction at 700 °C for 8 h

catalyst	D_p , nm ^a	S_{BET} , m ² /g	V_p , cm ³ /g	Ni ⁰ crystallite sizes (nm) ^b			particle size of Ni (nm) ^c	
				calcined	initial	8 h	initial	8 h
NiO–ZrO ₂	3	113	0.18		12	24	5–10	15–20
NiO–10Al ₂ O ₃ –ZrO ₂	6	86	0.25	10	12	11	5–10	10–15

^aThe pore diameter (D_p) and the pore volume (V_p) were determined by the BJH method, and the specific surface area (S_{BET}) was determined by the BET method. ^bThe Ni⁰ crystallite sizes was determined by XRD (Scherrer equation). ^cThe particle size of Ni was determined by TEM.

catalyst was stronger than that on the NiO–10Al₂O₃–ZrO₂ catalyst. There are three reasons. First, the C species determined by XPS could be affected by the polluted carbon that came from the oil in the pump. Second, the content of C species determined by XPS was the surface content, not the real value of carbon. The TGA presented the real value of carbon deposition. Lastly, the amorphous carbon formed in the pore of the NiO–10Al₂O₃–ZrO₂ catalyst, which cannot be detected by XPS, while more nanotube carbon formed on the surface of the NiO–ZrO₂ catalyst as proved by TEM, which was easily detected by XPS.^{37,38}

Those different types of carbon might play a role in the DRM reaction mechanisms. From the results of stability test, the reverse water-gas shift (RWGS) reaction occurred on the NiO–ZrO₂ catalyst. A part of CO₂ reacted with hydrogen rather than carbon, and thus this carbon may be transformed into an inactive carbon gradually and further into a type of coke that was very difficult to be removed, due to the accumulation, namely, graphite nanotubes of carbon.^{35,36} On the other hand, the CO₂ conversion (91 and 89% for 1 and 8 h, respectively) was slightly lower than CH₄ conversion (94 and 92% for 1 and 8 h, respectively) on the NiO–10Al₂O₃–ZrO₂ catalyst, which indicated that the rate of carbon deposition was higher than that of carbon elimination, thus leading to more carbon on the NiO–10Al₂O₃–ZrO₂ catalyst. Also, according to the results of TEM, the carbon on the NiO–10Al₂O₃–ZrO₂ catalyst was mainly the amorphous carbon.

Physicochemical Features of NiO–ZrO₂ and NiO–10Al₂O₃–ZrO₂ Catalysts. Figure 4 presented the adsorption/desorption isotherms of the non-promoted and promoted catalysts. The adsorption isotherms for NiO–10Al₂O₃–ZrO₂ and NiO–ZrO₂ catalysts were both type IV isotherms, with an H2 hysteresis loop according to the literature,³⁹ which is typical of mesoporous materials. The pore size distribution (Figure 4B) indicated that the pore size of NiO–ZrO₂ and NiO–10Al₂O₃–ZrO₂ catalysts is almost distributed at about 3 and 6 nm, respectively. The pore volume (V_p) and the specific surface area (S_{BET}) are listed in Table 3. A large pore volume (0.25 cm³/g)

and pore diameter (6 nm) were observed on the NiO–10Al₂O₃–ZrO₂ catalyst.

However, the specific surface area on the NiO–ZrO₂ catalyst was higher than the one on the NiO–10Al₂O₃–ZrO₂ catalyst. The specific surface area could be influenced by the pore volume, pore diameter, particle size, and so on. The large particle size of Ni species can lead to a lower surface area.^{29,40} The NiO species with the crystallite size of 10 nm (Table 3) could be detected on the NiO–10Al₂O₃–ZrO₂ catalyst, while almost no NiO species could be found on the NiO–ZrO₂ catalyst. Thus, the physical properties (pore volume and pore diameter) could be promoted by the introduction of aluminum. This large pore volume and pore diameter may cause an increase the proportion of metal nickel dispersed in the porous structure of the catalysts.

The reducibility of NiO–ZrO₂ and NiO–10Al₂O₃–ZrO₂ catalysts were determined by H₂-TPR experiments, as shown in Figure 5. The reduction temperatures on the NiO–10Al₂O₃–ZrO₂ catalyst shifted toward higher values as compared to the NiO–ZrO₂ catalyst, which was an indication for a stronger interaction between Ni and the support on the promoted catalyst. This stronger metal–support interaction could inhibit the sintering of Ni particles, hence enhancing the stability of the catalyst.⁴¹

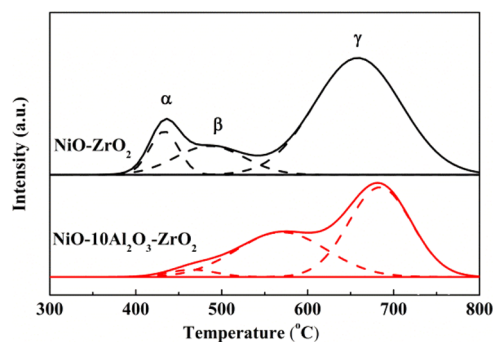


Figure 5. H₂-TPR profiles of NiO–ZrO₂ and NiO–10Al₂O₃–ZrO₂ catalysts.

Three peaks could be distinguished (denominated α , β , and γ) on both catalysts, and the content of each peak is presented in Table 4. The first peak (α) at 400–500 °C was related to the

Table 4. Consumption of H₂ and the Proportion of Three Peaks on the H₂-TPR Experiment

catalyst	total $\mu\text{mol H}_2/\text{g}$		H ₂ consumption (%)				ratio of out:in
			α		β		
	actual	theoretical	NiO	NiO	NiO	ZrO ₂	
NiO–ZrO ₂	626	468 ^a	9	15	51 ^b	25	24:51 ^c
NiO–10Al ₂ O ₃ –ZrO ₂	479	434	4	40	47	9	44:47

^aThe H₂ consumption of the theory calculated by ICP and the consumption of reduction of pure NiO. ^bThe proportion of NiO in the skeleton of ZrO₂. ^cThe ratio of the NiO species out:in of the skeleton.

reduction of NiO species with weak interaction between zirconia, which might be easy to sinter during the DRM reaction.^{42,43} The second peak (β) at 500–600 °C corresponded to the reduction of NiO species inside the mesoporous network with strong interaction between zirconium, which could maintain the original state even after reduction and reaction.^{44–46} The third peak (γ) at 600–800 °C was assigned to the NiO species in the skeleton of ZrO₂ and ZrO₂ species.^{47,48} The proportion of three peaks on NiO–10Al₂O₃–ZrO₂ and NiO–ZrO₂ catalysts is shown in Table 4. The content of the β peak was about 40% on the NiO–10Al₂O₃–ZrO₂ catalyst, which was higher than the one on the NiO–ZrO₂ catalyst (15%) because the NiO–10Al₂O₃–ZrO₂ catalyst exhibited a large pore volume and pore diameter. Considering the content of the α peak, about 44% (40 + 4 = 44%) H₂ consumption came from the reduction of NiO species out of the skeleton. The ratio of the NiO species out/in the skeleton was about 24:51 on NiO–ZrO₂ and 44:47 NiO–10Al₂O₃–ZrO₂ catalysts, respectively. In addition, a part of nickel species could be released and distributed on the surface of ZrO₂ or enter into the porosity. Then, this shift could lead to an increase in the proportion of NiO species on the surface, which could promote the activity of the catalyst, due to the probability of the contact of the reactant with the active metal. In addition, the total H₂ consumption on the NiO–10Al₂O₃–ZrO₂ catalyst was about 479 $\mu\text{mol H}_2/\text{g}$ (Table 4), which was higher than the theoretical value (434 $\mu\text{mol H}_2/\text{g}$), indicating that this 9% ((479 – 433)/479 × 100% = 9%) of H₂ consumption was assigned to the reduction of Zr⁴⁺ to Zr³⁺, as proved by Zr 3d of XPS profiles. As shown in Figure 8A and Table 5, the content of surface Zr⁴⁺ was 11 and 14% on NiO–ZrO₂ and NiO–10Al₂O₃–ZrO₂ catalysts, respectively. For the γ peak, except for the reduction of the ZrO₂ species, the rest was the contribution of NiO species. The proportion of NiO

in the γ peak was 51 and 47% on NiO–ZrO₂ and NiO–10Al₂O₃–ZrO₂ catalysts, respectively. This fact suggested that more NiO and ZrO₂ species were reduced on the NiO–ZrO₂ catalyst.

The morphology of reduced NiO–ZrO₂ and NiO–10Al₂O₃–ZrO₂ catalysts was determined by TEM, as shown in Figure 6. A similar distribution of nickel particles could be observed on both catalysts, almost at 5–10 nm. The highly dispersed Ni species on reduced catalysts could promote the activity of the DRM reaction. Herein, the similar distribution of Ni species resulted in similar initial activity on NiO–ZrO₂ and NiO–10Al₂O₃–ZrO₂ catalysts, which was consistent with the results of the activity test.

The crystallite sizes on NiO–ZrO₂ and NiO–10Al₂O₃–ZrO₂ catalysts were determined by XRD, as shown in Figure 7. The diffraction peak corresponding to NiO could not be observed on both catalysts after reduction, indicating that all the NiO species were reduced. Ni metal peaks were obvious on both catalysts before and after the reaction, and the crystallite size of Ni metal is shown in Table 3. Before the reaction, those two catalysts exhibited the same Ni⁰ crystallite size (12 nm), which was consistent with the TEM results. According to the H₂-TPR results, the NiO–ZrO₂ catalyst exhibited a higher content of the α peak (the NiO is well-known to be easily sintered) and lower content of the β peak (the NiO was more difficult to sinter), which led to very severe sintering. Therefore, the Ni metal particle size increased to 24 nm on the NiO–ZrO₂ catalyst after the reaction, which corresponded to the nickel particle size determined by the TEM experiment, concentrated at 15–20 nm (Table 3). On the contrary, it decreased to 11 nm on NiO–10Al₂O₃–ZrO₂ catalyst after reaction, and according to the TEM results, the nickel particle size mainly distributed at 10–15 nm. The lower content of the α peak and higher content of the β peak formed on the NiO–10Al₂O₃–ZrO₂ catalyst, and thus, the Ni species might be better to stay pristine in the porosity, as compared with the NiO–ZrO₂ catalyst. There were two reasons to explain the decrease of the Ni metal particle size. First, the Ni metal can be redispersed during reaction. Second, part of metallic Ni (Ni⁰) could be oxidized to NiO or NiCO_x by CO, and CO₂ could be adsorbed on Ni⁰.^{30,49–51}

Obviously, the structure of the nickel particle on the NiO–10Al₂O₃–ZrO₂ catalyst was more stable, contributing to the stability of the catalyst. Therefore, the NiO–10Al₂O₃–ZrO₂ catalyst exhibited higher stability for the dry reforming of methane. In addition, the large nickel metal particle size could affect the selectivity of catalyst toward carbon deposition.^{52,53} Hence, the carbon deposited on the NiO–ZrO₂ catalyst was difficult to be removed because of its graphite form.

From XPS, the Zr 3d in XPS profiles of NiO–10Al₂O₃–ZrO₂ and NiO–ZrO₂ catalysts before and after reduction were studied and the results are presented in Figure 8A. The intensity of the surface Zr species decreased on both catalysts after the reaction because the formation of carbon would cover on the

Table 5. Content of Zr, Ni, and O Species on both Catalysts before and after Reaction at 700 °C for 8 h, Determined by XPS

catalyst	Zr proportion (%)						Ni content (wt %)						O ²⁻ /O _{ads}	
	initial		8 h				initial		8 h				initial	8 h
	Zr ⁴⁺	Zr ³⁺	Zr ⁴⁺	Zr ³⁺	Zr ²⁺	Zr ¹⁺	Ni	Ni ⁰	Ni	Ni ⁰	ΔNpi^a	ΔNi^{0b}		
NiO–ZrO ₂	11	89	17	25	23	35	5.6	1.9	4.4	1.1	–21%	–42%	0.98	0.27
NiO–10Al ₂ O ₃ –ZrO ₂	14	86	22	34	44		5.8	1.0	5.6	1.1	–3%	+10%	1.02	0.94

^aThe loss of surface nickel species after the DRM reaction for 8 h. ^bThe loss of surface nickel metal species after the DRM reaction for 8 h.

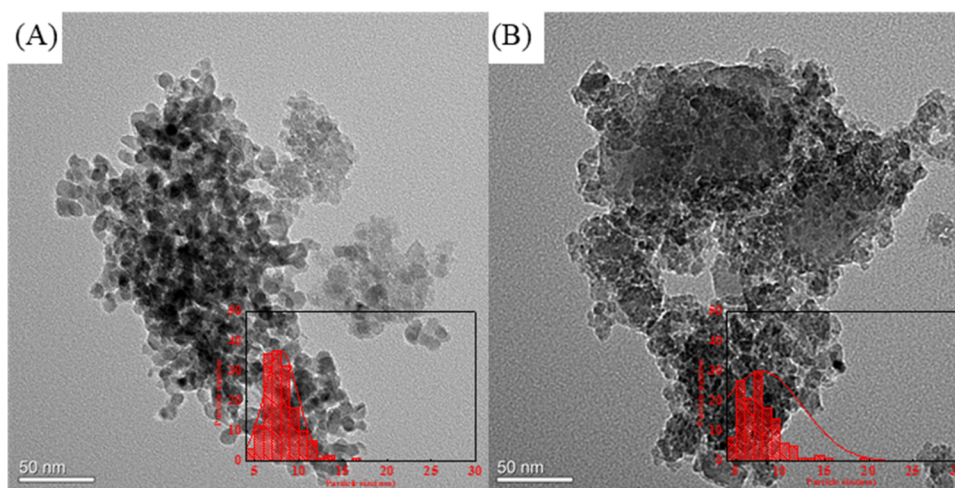


Figure 6. Morphology of reduced NiO–ZrO₂ (A) and reduced NiO–10Al₂O₃–ZrO₂ (B) catalysts determined by TEM.

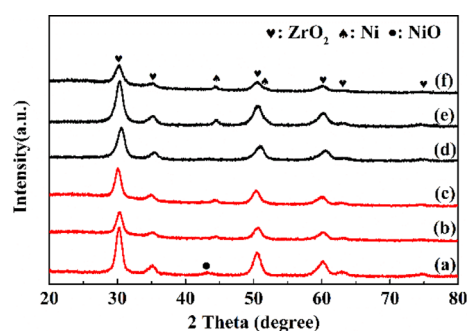


Figure 7. XRD profiles of (a) NiO–ZrO₂ and (b) NiO–10Al₂O₃–ZrO₂ catalysts and (c) NiO–ZrO₂ and (d) NiO–10Al₂O₃–ZrO₂ catalysts after reduction at 700 °C for 1 h and (e) NiO–ZrO₂ and (f) NiO–10Al₂O₃–ZrO₂ catalysts after reaction at 700 °C for 8 h.

surface of catalyst, especially for the NiO–ZrO₂ catalyst. More surface carbon formed on the NiO–ZrO₂ catalyst, as proved by C 1s in XPS. Similar results had been reported in the literature.^{54,55} The peaks at about 182.3, 181.4, 180.5, and 179.3 eV are attributed to the Zr⁴⁺, Zr³⁺, Zr²⁺, and Zr¹⁺, respectively.^{47,56–60} The proportion of Zr⁴⁺ and Zr³⁺ is listed at Table 5. The proportion of surface Zr⁴⁺ on NiO–ZrO₂ and NiO–10Al₂O₃–ZrO₂ catalysts were 11 and 14%, respectively, which indicated that a part of Zr⁴⁺ could be reduced to Zr³⁺ after reduction on both catalysts. After the reaction, a part of surface Zr³⁺ species was reduced to lower valence, e.g., Zr²⁺ and Zr¹⁺.^{57–60} Then, the NiO–ZrO₂ catalyst exhibited a higher content of lower valence zirconium, especially containing Zr¹⁺ species of 35%, while no Zr¹⁺ species could be observed on the NiO–10Al₂O₃–ZrO₂ catalyst, manifesting that the structure of ZrO₂ might be more stable by the modification of Al.

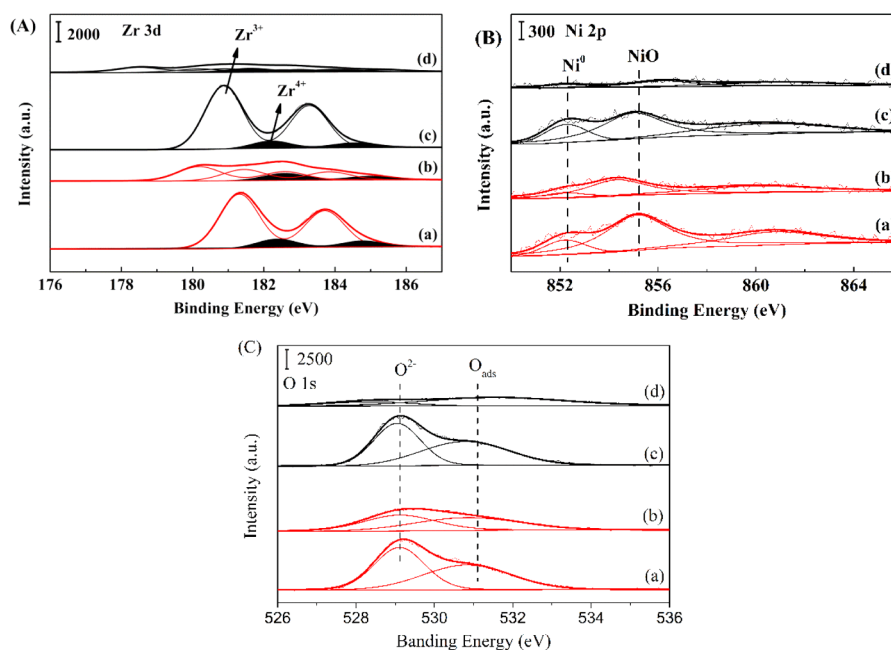


Figure 8. Zr 3d (A), Ni 2p (B), and O 1s (C) profiles of (a) NiO–10Al₂O₃–ZrO₂ and (c) NiO–ZrO₂ catalysts after reduction at 700 °C for 1 h and (b) NiO–10Al₂O₃–ZrO₂ and (d) NiO–ZrO₂ catalysts after reaction at 700 °C for 8 h.

We also followed the Ni species at the surface by XPS. Figure 8B presented the Ni 2p profiles of NiO–10Al₂O₃–ZrO₂ and NiO–ZrO₂ catalysts before and after the reaction. The peak at about 852.8 eV was attributed to Ni⁰ species, while another peak was assigned to NiO species.³⁶ After the reaction (DRM, 700 °C, 8 h), the NiO peak shifted slightly to lower binding energy on NiO–10Al₂O₃–ZrO₂. It suggested that the electrons on the support could transfer to Ni species during the reaction, which might contribute to the catalytic performance of the catalyst.^{36,53} Whereas, the NiO peak shifted slightly to higher binding energy on the NiO–ZrO₂ catalyst, which indicated that the ability of nickel species to receive electrons on the NiO–10Al₂O₃–ZrO₂ catalyst was weaker than the one on the NiO–ZrO₂ catalyst.^{36,53} Except for the electron transfer, the nickel content also varied visibly. Before the reaction, the content of surface nickel species on NiO–ZrO₂ catalyst was about 5.6 wt %, while after reaction for 8 h, it decreased by 24% (Table S). A larger amount of reduction could be observed in the content of surface Ni⁰ species. It decreased by 42% after reaction. Thus, the activity on the NiO–ZrO₂ catalyst also decreased. However, nickel species were relatively stable on the NiO–10Al₂O₃–ZrO₂ catalyst after the reaction, the surface nickel content was 5.8 wt % at the beginning, while it just decreased by 3% after reaction for 8 h.

Meanwhile, the initial content of surface Ni⁰ species was about 1.0 wt % and increased by 10% on the NiO–10Al₂O₃–ZrO₂ catalyst after reaction for 8 h. The content of nickel species at the surface of the NiO–10Al₂O₃–ZrO₂ catalyst was more stable than that on the NiO–ZrO₂ catalyst, which might contribute to the stability of the catalyst. Therefore, the NiO–10Al₂O₃–ZrO₂ catalyst exhibited higher stability for the dry reforming of methane. After reduction, a large amount of NiO species could be detected, which may be explained by the following three reasons. First of all, Ni⁰ species on the surface of the catalyst could adsorb the oxygen in the air; second, the Ni⁰ species may be re-oxidized when the reduced catalyst exposed to air; and the last, it could be due to the strong interaction between the metal and support.^{31,61}

The O 1s in XPS profiles of NiO–10Al₂O₃–ZrO₂ and NiO–ZrO₂ catalysts before and after the reaction was studied, and the results are presented in Figure 8C. The peaks at 529.0 and 531.2 eV were assigned to the lattice oxygen species (O²⁻) and adsorbed oxygen species (O_{ads}), respectively.^{3,29,62,63} The ratio of O²⁻/O_{ads} is listed in Table 5. After reduction, the ratio of O²⁻/O_{ads} on NiO–ZrO₂ and NiO–10Al₂O₃–ZrO₂ catalysts was almost the same. After reaction, it decreased from 0.98 to 0.27 on the NiO–ZrO₂ catalyst, while it decreased from 1.02 to 0.94 on the NiO–10Al₂O₃–ZrO₂ catalyst. This phenomenon implied that the surface lattice oxygen species on the NiO–ZrO₂ catalyst plummeted, which was consistent with that more Zr species were reduced after the reaction on the NiO–ZrO₂ catalyst.

The ammonia desorption results are shown in Figure 9. A wide composite desorption peak with the temperature range of 50 to 500 °C was obtained on both NiO–ZrO₂ and NiO–10Al₂O₃–ZrO₂ catalysts. According to the literature,^{64,65} the wide peak could be deconvoluted into three contributions, which corresponds to weak, medium strength, and strong acid sites. The medium strength and strong peaks shifted to higher temperatures on the NiO–10Al₂O₃–ZrO₂ catalyst. In other words, the presence of Al seems generally to enhance the acidity of the catalyst. The deconvolution results of the NH₃-TPD profiles are presented in Table 6. The total acidity on NiO–10Al₂O₃–ZrO₂ and NiO–ZrO₂ catalysts was 466 and 486 μmol

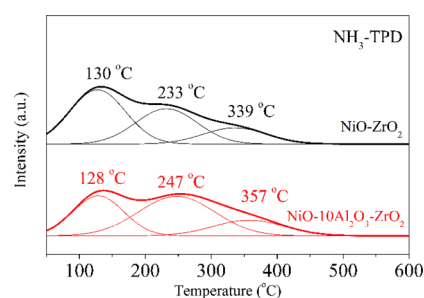


Figure 9. NH₃-TPD profiles of NiO–ZrO₂ and NiO–10Al₂O₃–ZrO₂ catalysts.

NH₃/g, respectively. In addition, the proportion of weak, medium strength, and strong acid sites on the NiO–ZrO₂ catalyst was 48.5, 34.9, and 16.6%, respectively. It was 26.9, 43.7, and 29.4% for weak, medium strength, and strong acid sites on the NiO–10Al₂O₃–ZrO₂ catalyst, respectively. The NiO–ZrO₂ catalyst exhibited a higher proportion of weak acid sites, while the NiO–10Al₂O₃–ZrO₂ catalyst presented a higher proportion of medium strength and strong acid sites. Generally, the acidity could result in carbon deposition in the dry reforming of methane.⁶⁶ The strong acid sites were considered important in the activation of hydrocarbons, and thus, the catalyst with more strong acid sites would promote the activation of methane.⁶⁷ As a consequence, the NiO–10Al₂O₃–ZrO₂ catalyst exhibited higher methane conversion and carbon deposition.

The FT-IR spectra of the adsorption of CO over NiO–ZrO₂ and NiO–10Al₂O₃–ZrO₂ catalysts before and after the reaction are shown in Figure 10. The band at 2172 cm⁻¹ was ascribed to CO interaction with Zr⁴⁺ moieties, and the signal at 2115 cm⁻¹ was attributed to the physisorbed CO species.^{68–70} The intensity of those two peaks became weak when the temperature increased to 200 °C. In addition, two IR bands at 1638 and 1870 cm⁻¹ could be observed on reduced NiO–ZrO₂ and NiO–10Al₂O₃–ZrO₂ catalysts, which were assigned to CO species adsorbed on Ni metal particles.^{68,71} Both peaks on NiO–ZrO₂ catalysts disappeared when the temperature increased to 200 °C, while the band at 1638 cm⁻¹ on the NiO–10Al₂O₃–ZrO₂ catalyst shifted to lower frequencies (1612 cm⁻¹). This red shift was caused by the decreasing of oxygen concentration on the interface of metal and support due to the desorption of CO species.^{72,73} A similar phenomenon could be observed on used NiO–ZrO₂ and NiO–10Al₂O₃–ZrO₂ catalysts. In addition, no IR band at 1870 cm⁻¹ could be observed on used catalysts. In all, the CO species were preferentially interacted with metallic Ni species on the NiO–10Al₂O₃–ZrO₂ catalyst, which might contribute the promotion effect activity for dry reforming of methane.

The aluminum could be embedded into the skeleton of zirconia during the synthesis of the NiO–10Al₂O₃–ZrO₂ catalyst, which could then modify the structure of the NiO–ZrO₂ catalyst from three aspects: First, the introduction of Al increases the pore volume (0.25 cm³/g) and pore diameter (6 nm). The larger pore volume can accommodate higher content of nickel species and the larger pore diameter can restrict grain growth due to the strong interaction, thereby enhancing the dispersion. Second, the addition of Al could inhibit the reduction of the zirconia species, resulting in less Zr⁴⁺ species being reduced under the condition of reduction and reaction. Third, the promotion by Al enhances the interaction between nickel and the support, which could restrain the sintering and the

Table 6. Deconvolution of the NH₃-TPD Profiles Obtained for the NiO–ZrO₂ and NiO–10Al₂O₃–ZrO₂ Catalysts

catalyst	NH ₃ desorbed (%)						total acidity (μmol NH ₃ /g)
	weak		medium strength		strong		
	position (°C)	proportion (%)	position (°C)	proportion (%)	position (°C)	proportion (%)	
NiO–ZrO ₂	130	48.5	233	34.9	339	16.6	486
NiO–10Al ₂ O ₃ –ZrO ₂	128	26.9	247	43.7	357	29.4	466

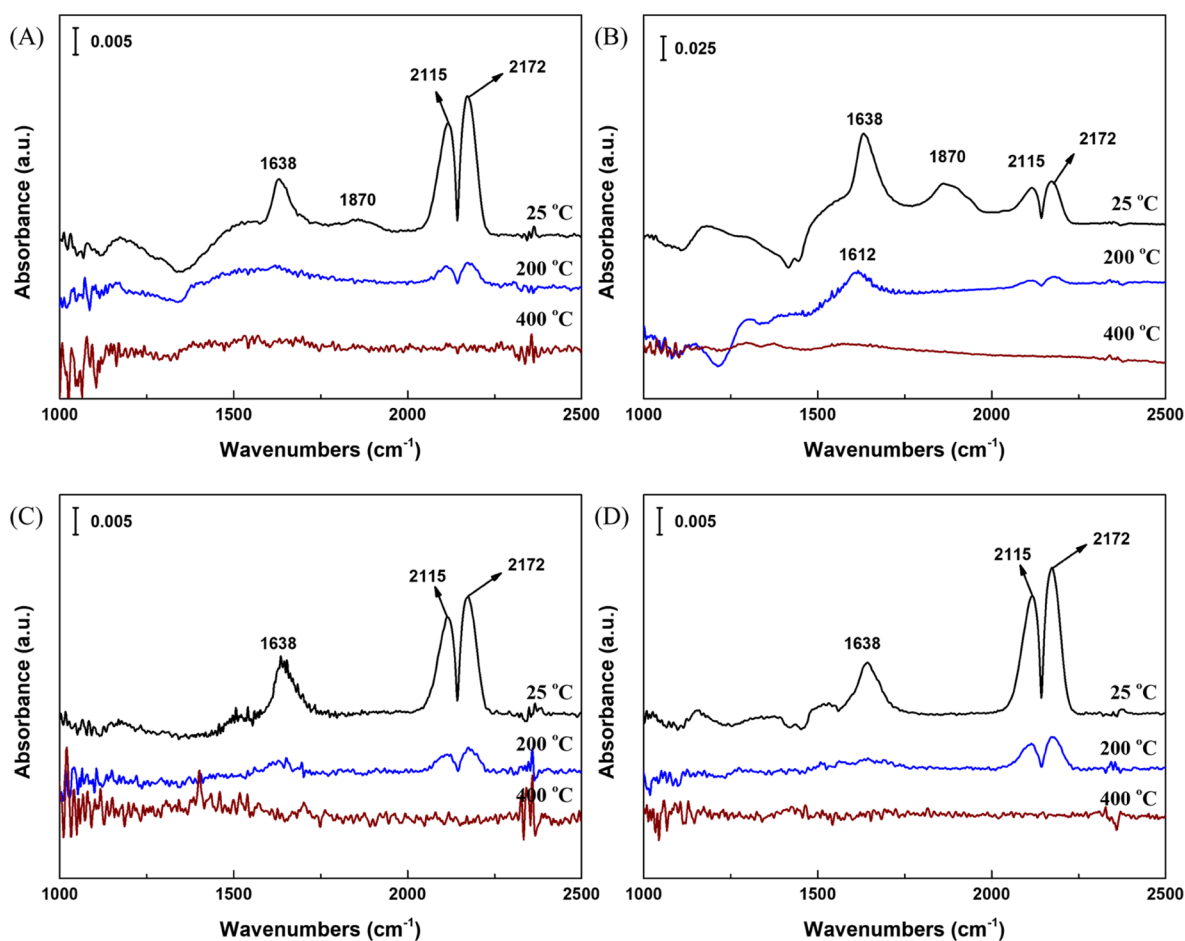


Figure 10. FT-IR-CO experiment for reduced NiO–ZrO₂ (A) and NiO–10Al₂O₃–ZrO₂ (B) catalysts and used NiO–ZrO₂ (C) and used NiO–10Al₂O₃–ZrO₂ (D).

loss of nickel during the DRM reaction, thereby promoting the stability of the catalyst.

CONCLUSIONS

In this study, we clearly showed that aluminum (Al), as promoter could enhance the activity, selectivity, and stability of the NiO–ZrO₂ catalyst for dry reforming of methane. The activity tests were conducted from 550 to 800 °C, and the NiO–10Al₂O₃–ZrO₂ catalyst exhibited the highest catalytic performance for dry reforming of methane at lower temperature.

Furthermore, the stability tests, carried out at 700 °C for 8 h, showed that the NiO–10Al₂O₃–ZrO₂ catalyst presented higher activity, selectivity, and stability than those on the NiO–ZrO₂ catalyst. This high activity was directly linked to the higher content at surface of nickel particles and the smaller particle size, which was attributed to the larger pore volume and pore diameter on the NiO–10Al₂O₃–ZrO₂ catalyst.

Therefore, the NiO–10Al₂O₃–ZrO₂ catalyst exhibited higher stability for the DRM reaction. In fact, after 8 h runs, on the

NiO–10Al₂O₃–ZrO₂ catalyst, it formed coke that is easier to be eliminated as a form of amorphous and disordered carbon (C–O and C=O species). Also, on the NiO–ZrO₂ catalyst, a severe metal sintering occurred and more nanotube carbon (graphite) formed, which was very difficult to be removed.

EXPERIMENTAL SECTION

Synthesis of a Series of 10NiO–xAl₂O₃–(90 – x)ZrO₂ Catalysts. At the First, the dissolution of Pluronic P123 (amphiphilic block copolymer), Ni(NO₃)₂·6H₂O, Zr(NO₃)₂·xH₂O, CH₄N₂O, and C₉H₂₁AlO₃ in 375 mL distilled water was carried out to obtain a mixture slurry under vigorous stirring. The concentration of the Ni(NO₃)₂ solution was about 0.01 mol/L. The molar ratio of Ni, Al, and Zr was 10:x:90 – x (x = 0, 10, 20, 45, 90), respectively. Second, the obtained suspension was heated to 95 °C under vigorous stirring for 2 days to ensure that the suspension was precipitated completely. Next, the suspension was subsequently aged at 100 °C for 1 day since the aging process could increase the average particle size and particle

size distribution.⁷⁴ After filtering under vacuum suction, washing by little distilled water for three times, and drying at 25 °C, the obtained precursor was calcined at 800 °C for 300 min with the heating rate of 1 °C/min. Last, the green powder samples were denoted as NiO–ZrO₂, NiO–10Al₂O₃–ZrO₂, NiO–20Al₂O₃–ZrO₂, and NiO–45Al₂O₃–ZrO₂, NiO–Al₂O₃, respectively.

Dry Reforming Catalytic Test. The dry reforming activity test was conducted with the temperature range from 550 to 800 °C (interval of each 50 °C with 30 min to reach the steady state) in a flow type U microreactor. A thermocouple (Type K) was placed near to the catalytic bed to monitor the reaction temperature for each test. The mixture of reactant gases with a molar composition of CO₂:CH₄:Ar = 1:1:8 corresponding to the total gas hourly space velocity of 48,000 h⁻¹ was introduced. For time on stream catalytic tests, the same reactant gases were introduced through the catalytic bed held at 700 °C for 8 h. Prior to each DRM reaction, the catalysts were reduced at the same temperature for 60 min in the gas stream of 5 vol % H₂ in Ar. The outgases were detected by a gas micro chromatography equipped with a TCD detector to analyze the composition of products. The calculation of conversions of CH₄ and CO₂ and H₂/CO was described elsewhere.⁴⁷ The experimental error was ±5%.

Catalyst Characterization. Textural properties were determined by the nitrogen adsorption desorption measurements in a Belsorp Mini II instrument at -196 °C. Prior to measurement, the catalysts were pretreated under a vacuum condition at 200 °C for 120 min. The phase structure of the catalysts was evaluated by XRD (X-ray diffraction) analysis on a diffractometer of DX-1000 CSC using a source of Cu K α X-ray. The data was collected in the 2 θ range of 10–80°. The scan step size was 0.03°. The reducibility of catalysts was determined by the H₂-TPR (temperature-programmed reduction of H₂) on a BELCAT-M instrument. The mass of catalyst was about 60 mg. Before the test, the catalyst was cleaned at 150 °C under helium flow for 30 min. Then, the sample was reduced under a mixture flow of 5 vol % H₂ in Ar with a heating rate (10 °C/min) from 100 to 900 °C. The surface elements of catalysts were characterized by XPS (X-ray photoelectron spectroscopy) analysis, which was carried out on a KRATOS spectrometer instrument with monochromated Al radiation. All of the data (the electron binding energy) were referenced to the C 1s peak at 284.5 eV.²⁹ The morphology of catalysts was determined by TEM (transmission electron microscopy) experiments, which was conducted on the FEI Tecnai G2 20 Twin apparatus. The coke of used catalysts was obtained by TGA (thermogravimetric analysis). The mass of the sample was 10 mg. The sample was heated from 30 to 800 °C with a 5 °C·min⁻¹ rate under air of 60 mL·min⁻¹. Raman spectroscopy experiments were conducted on an objective of X50LWD with a laser of 532.17 nm, a grating of 600 gr/mm, a filter of D1, and a hole of 200 μ m. The data was collected from the wavenumber values of 40–4000 cm⁻¹. Herein, Raman characterization was carried out for the in-depth study of carbon species deposited on the used catalysts.^{33,34} The temperature-programmed desorption of NH₃ (NH₃-TPD) method was carried out using a BELCAT-M instrument. Before the test, the sample (60 mg) was reduced at 700 °C under a mixture flow of 5 vol % H₂ in Ar and then cooled down to 50 °C under He flow. Next, NH₃ was adsorbed under 10% NH₃/He flow for 1 h. After cleaning the weakly adsorbed NH₃ on the surface of the sample for 30 min, the material was heated from 50 to 800 °C under He flow with a 10 °C/min heating rate. The outgas was detected by a TCD detector. The CO adsorption FT-

IR experiments were carried out on a Bruker infrared spectrometer (FT-IR V70). Before the test, the sample was pretreated at 700 °C under the same condition as the activity test and then cooled down to room temperature. The CO was adsorbed in the dilute feed gas (10% CO) for 1 h at 25 °C. Then, the sample was heated to 400 °C under Ar flow.

AUTHOR INFORMATION

Corresponding Authors

Patrick Da. Costa – Sorbonne Université, Saint-Cyr-L'Ecole 78210, France; orcid.org/0000-0002-0083-457X; Email: patrick.da_costa@sorbonne-universite.fr

Changwei Hu – College of Chemical Engineering, Sichuan University, Chengdu, Sichuan 610065, P. R. China; Key Laboratory of Green Chemistry and Technology, Ministry of Education, College of Chemistry, Sichuan University, Chengdu, Sichuan 610064, P. R. China; orcid.org/0000-0002-4094-6605; Email: changwei.hu@scu.edu.cn

Authors

Ye Wang – College of Chemical Engineering, Sichuan University, Chengdu, Sichuan 610065, P. R. China; Sorbonne Université, Saint-Cyr-L'Ecole 78210, France

Yannan Wang – Key Laboratory of Green Chemistry and Technology, Ministry of Education, College of Chemistry, Sichuan University, Chengdu, Sichuan 610064, P. R. China

Li Li – Key Laboratory of Green Chemistry and Technology, Ministry of Education, College of Chemistry, Sichuan University, Chengdu, Sichuan 610064, P. R. China

Chaojun Cui – College of Chemical Engineering, Sichuan University, Chengdu, Sichuan 610065, P. R. China

Xudong Liu – Key Laboratory of Green Chemistry and Technology, Ministry of Education, College of Chemistry, Sichuan University, Chengdu, Sichuan 610064, P. R. China

Complete contact information is available at:
<https://pubs.acs.org/10.1021/acsomega.1c03174>

Author Contributions

Y.W. did the conceptualization, investigation, formal analysis, writing of the original draft, review, and editing. Y.W., L.L., C.C., and X.L. did the investigation, writing of the review, and editing. P.D.C. did the conceptualization, supervision, writing of the review, and editing. C.H. did the conceptualization, supervision, writing of the review, and editing.

Funding

This work was supported by the National Key R&D Program of China (2018YFB1501404), the 111 program (B17030), and Fundamental Research Funds for the Central Universities.

Notes

The authors declare no competing financial interest.

ACKNOWLEDGMENTS

Y.W. acknowledges the financial support of CSC (China Scholarship Council) for her joint-PhD research in Sorbonne Université. We thank Yunfei Tian of the analytical & testing center of Sichuan University for XPS experiments.

REFERENCES

(1) Jang, W. J.; Shim, J. O.; Kim, H. M.; Yoo, S. Y.; Roh, H.-S. A review on dry reforming of methane in aspect of catalytic properties. *Catal. Today* **2019**, *324*, 15–26.

- (2) Wang, Y.; Yao, L.; Wang, S.; Mao, D.; Hu, C. Low-temperature catalytic CO₂ dry reforming of methane on Ni-based catalysts: a review. *Fuel Process. Technol.* **2018**, *169*, 199–206.
- (3) Zhang, M.; Zhang, J.; Wu, Y.; Pan, J.; Zhang, Q.; Tan, Y.; Han, Y. Insight into the effects of the oxygen species over Ni/ZrO₂ catalyst surface on methane reforming with carbon dioxide. *Appl. Catal., B* **2019**, *244*, 427–437.
- (4) Nikoo, M. K.; Amin, N. A. S. Thermodynamic analysis of carbon dioxide reforming of methane in view of solid carbon formation. *Fuel Process. Technol.* **2011**, *92*, 678–691.
- (5) Arora, S.; Prasad, R. An overview on dry reforming of methane: strategies to reduce carbonaceous deactivation of catalysts. *RSC Adv.* **2016**, *6*, 108668–108688.
- (6) Pakhare, D.; Spivey, J. A review of dry (CO₂) reforming of methane over noble metal catalysts. *Chem. Soc. Rev.* **2014**, *43*, 7813–7837.
- (7) Singh, S. A.; Madras, G. Sonochemical synthesis of Pt, Ru doped TiO₂ for methane reforming. *Appl. Catal., A* **2016**, *518*, 102–114.
- (8) Moral, A.; Reyero, I.; Alfaro, C.; Bimbela, F.; Gandía, L. M. Syngas production by means of biogas catalytic partial oxidation and dry reforming using Rh-based catalysts. *Catal. Today* **2018**, *299*, 280–288.
- (9) Pompeo, F.; Nichio, N. N.; Souza, M. M. V. M.; Cesar, D. V.; Ferretti, O. A.; Schmal, M. Study of Ni and Pt catalysts supported on α -Al₂O₃ and ZrO₂ applied in methane reforming with CO₂. *Appl. Catal., A* **2007**, *316*, 175–183.
- (10) Polo-Garzon, F.; Pakhare, D.; Spivey, J. J.; Bruce, D. A. Dry reforming of methane on Rh-doped pyrochlore catalysts: A steady-state isotopic transient kinetic study. *ACS Catal.* **2016**, *6*, 3826–3833.
- (11) Albarazi, A.; Beaunier, P.; Da Costa, P. Hydrogen and syngas production by methane dry reforming on SBA-15 supported nickel catalysts: On the effect of promotion by Ce_{0.75}Zr_{0.25}O₂ mixed oxide. *Int. J. Hydrogen Energy* **2013**, *38*, 127–139.
- (12) Wang, F.; Han, B.; Zhang, L.; Xu, L.; Yu, H.; Shi, W. CO₂ reforming with methane over small-sized Ni@SiO₂ catalysts with unique features of sintering-free and low carbon. *Appl. Catal., B* **2018**, *235*, 26–35.
- (13) Han, J. W.; Kim, C.; Park, J. S.; Lee, H. Highly coke-resistant Ni nanoparticle catalysts with minimal sintering in dry reforming of methane. *ChemSusChem* **2014**, *7*, 451–456.
- (14) Liu, H.; Hadjltaief, H. B.; Benzina, M.; Gálvez, M. E.; Da Costa, P. Natural clay based nickel catalysts for dry reforming of methane: On the effect of support promotion (La, Al, Mn). *Int. J. Hydrogen Energy* **2019**, *44*, 246–255.
- (15) Talkhoncheg, S. K.; Haghghi, M. Syngas production via dry reforming of methane over Ni-based nanocatalyst over various supports of clinoptilolite, ceria and alumina. *J. Nat. Gas Sci. Eng.* **2015**, *23*, 16–25.
- (16) Wei, J.-M.; Xu, B.-Q.; Li, J.-L.; Cheng, Z.-X.; Zhu, Q.-M. Highly active and stable Ni/ZrO₂ catalyst for syngas production by CO₂ reforming of methane. *Appl. Catal., A* **2000**, *196*, L167–L172.
- (17) Verykios, X. E. Catalytic dry reforming of natural gas for the production of chemicals and hydrogen. *Int. J. Hydrogen Energy* **2003**, *28*, 1045–1063.
- (18) Lou, Y.; Steib, M.; Zhang, Q.; Tiefenbacher, K.; Horváth, A.; Jentys, A.; Liu, Y.; Lercher, J. A. Design of stable Ni/ZrO₂ catalysts for dry reforming of methane. *J. Catal.* **2017**, *356*, 147–156.
- (19) Kumar, P.; Sun, Y.; Idem, R. O. Nickel-based ceria, zirconia, and ceria–zirconia catalytic systems for low-temperature carbon dioxide reforming of methane. *Energy Fuels* **2007**, *21*, 3113–3123.
- (20) Sajjadi, S. M.; Haghghi, M.; Rahmani, F. Sol–gel synthesis of Ni–Co/Al₂O₃–MgO–ZrO₂ nanocatalyst used in hydrogen production via reforming of CH₄/CO₂ greenhouse gases. *J. Nat. Gas Sci. Eng.* **2015**, *22*, 9–21.
- (21) Barroso-Quiroga, M. M.; Castro-Luna, A. E. Catalytic activity and effect of modifiers on Ni-based catalysts for the dry reforming of methane. *Int. J. Hydrogen Energy* **2010**, *35*, 6052–6056.
- (22) Sokolov, S.; Kondratenko, E. V.; Pohl, M. M.; Barkschat, A.; Rodemerck, U. Stable low-temperature dry reforming of methane over mesoporous La₂O₃–ZrO₂ supported Ni catalyst. *Appl. Catal., B* **2012**, *113–114*, 19–30.
- (23) Miao, Z.; Li, Z.; Suo, C.; Zhao, J.; Si, W.; Zhou, J.; Zhuo, S. One-pot synthesis of Al₂O₃ modified mesoporous ZrO₂ with excellent thermal stability and controllable crystalline phase. *Adv. Powder Technol.* **2018**, *29*, 3569–3576.
- (24) Therdthianwong, S.; Therdthianwong, A.; Siangchin, C.; Yongprapat, S. Synthesis gas production from dry reforming of methane over Ni/Al₂O₃ stabilized by ZrO₂. *Int. J. Hydrogen Energy* **2008**, *33*, 991–999.
- (25) Therdthianwong, S.; Siangchin, C.; Therdthianwong, A. Improvement of coke resistance of Ni/Al₂O₃ catalyst in CH₄/CO₂ reforming by ZrO₂ addition. *Fuel Process. Technol.* **2008**, *89*, 160–168.
- (26) Souza, M. M. V. M.; Aranda, D. A. G.; Schmal, M. Reforming of methane with carbon dioxide over Pt/ZrO₂/Al₂O₃ catalysts. *J. Catal.* **2001**, *204*, 498–511.
- (27) Li, H.; Wang, J. Study on CO₂ reforming of methane to syngas over Al₂O₃–ZrO₂ supported Ni catalysts prepared via a direct sol–gel process. *Chem. Eng. Sci.* **2004**, *59*, 4861–4867.
- (28) Chai, R.; Li, Y.; Zhang, Q.; Zhao, G.; Liu, Y.; Lu, Y. Monolithic Ni–MO_x/Ni-foam (M= Al, Zr or Y) catalysts with enhanced heat/mass transfer for energy-efficient catalytic oxy-methane reforming. *Catal. Commun.* **2015**, *70*, 1–5.
- (29) Wang, Y.; Zhao, Q.; Wang, Y.; Hu, C.; Da Costa, P. One-step synthesis of highly active and stable Ni–ZrO_x for dry reforming of methane. *Ind. Eng. Chem. Res.* **2020**, *59*, 11441–11452.
- (30) Swirk, K.; Gálvez, M. E.; Motak, M.; Grzybek, T.; Rønning, M.; Da Costa, P. Yttrium promoted Ni-based double-layered hydroxides for dry methane reforming. *J. CO₂ Util.* **2018**, *27*, 247–258.
- (31) Yao, L.; Wang, Y.; Shi, J.; Xu, H.; Shen, W.; Hu, C. The influence of reduction temperature on the performance of ZrO_x/Ni–MnO_x/SiO₂ catalyst for low-temperature CO₂ reforming of methane. *Catal. Today* **2016**, *281*, 259–267.
- (32) Pechimuthu, N. A.; Pant, K. K.; Dhingra, S. C. Deactivation studies over Ni–K/CeO₂–Al₂O₃ catalyst for dry reforming of methane. *Ind. Eng. Chem. Res.* **2007**, *46*, 1731–1736.
- (33) Bai, T.; Zhang, X.; Wang, F.; Qu, W.; Liu, X.; Duan, C. Coking behaviors and kinetics on HZSM-5/SAPO-34 catalysts for conversion of ethanol to propylene. *J. Energy Chem.* **2016**, *25*, 545–552.
- (34) McFarlane, A. R.; Silverwood, I. P.; Norris, E. L.; Ormerod, R. M.; Frost, C. D.; Parker, S. F.; Lennon, D. The application of inelastic neutron scattering to investigate the steam reforming of methane over an alumina-supported nickel catalyst. *Chem. Phys.* **2013**, *427*, 54–60.
- (35) Kumar, N.; Wang, Z.; Kanitkar, S.; Spivey, J. J. Methane reforming over Ni-based pyrochlore catalyst: deactivation studies for different reactions. *Appl. Petrochem. Res.* **2016**, *6*, 201–207.
- (36) Wang, Y.; Yao, L.; Wang, Y.; Wang, S.; Zhao, Q.; Mao, D.; Hu, C. Low-temperature catalytic CO₂ dry reforming of methane on Ni–Si/ZrO₂ catalyst. *ACS Catal.* **2018**, *8*, 6495–6506.
- (37) Nuernberg, G. B.; Fajardo, H. V.; Mezalira, D. Z.; Casarin, T. J.; Probst, L. F. D.; Carreño, N. L. V. Preparation and evaluation of Co/Al₂O₃ catalysts in the production of hydrogen from thermo-catalytic decomposition of methane: Influence of operating conditions on catalyst performance. *Fuel* **2008**, *87*, 1698–1704.
- (38) Jeong, S. H.; Hwang, H. Y.; Hwang, S. K.; Lee, K. H. Carbon nanotubes based on anodic aluminum oxide nano-template. *Carbon* **2004**, *42*, 2073–2080.
- (39) Singh, K. S. W.; Rouquerol, J.; Bergeret, G.; Gallezot, P.; Vaarkamp, M.; Koningsberger, D. C.; Datye, A. K.; Niemantsverdriet, J. W.; Butz, T.; Engelhardt, G.; Mestl, G.; Knözinger, H.; Jobic, H. Characterization of Solid Catalysts: Sections 3.1.1–3.1.3. In *Handbook of heterogeneous catalysis*; VCH Verlagsgesellschaft mbH, 1997, 427–582; DOI: 10.1002/9783527619474.
- (40) Rezaei, M.; Alavi, S. M.; Sahebdehfar, S.; Xinmei, L.; Qian, L.; Yan, Z.-F. CO₂–CH₄ Reforming over Nickel Catalysts Supported on Mesoporous Nanocrystalline Zirconia with High Surface Area. *Energy Fuels* **2007**, *21*, 581–589.
- (41) Corthals, S.; Van Nederkassel, J.; Geboers, J.; De Winne, H.; Van Noyen, J.; Moens, B.; Sels, B.; Jacobs, P. Influence of composition of MgAl₂O₄ supported NiCeO₂ZrO₂ catalysts on coke formation and

catalyst stability for dry reforming of methane. *Catal. Today* **2008**, *138*, 28–32.

(42) Cai, M.; Wen, J.; Chu, W.; Checong, X.; Li, Z. Methanation of carbon dioxide on Ni/ZrO₂-Al₂O₃ catalysts: Effects of ZrO₂ promoter and preparation method of novel ZrO₂-Al₂O₃ carrier. *J. Nat. Gas Chem.* **2011**, *20*, 318–324.

(43) Wang, H. W.; Wu, J. X.; Wang, X. Y.; Wang, H.; Liu, J. R. Formation of perovskite-type LaNiO₃ on La-Ni/Al₂O₃-ZrO₂ catalysts and their performance for CO methanation. *J. Fuel Chem. Technol.* **2021**, *49*, 186–197.

(44) Fakeeha, A. H.; Arafat, Y.; Ibrahim, A. A.; Shaikh, H.; Atia, H.; Abasaed, A. E.; Armbruster, U.; Al-Fatesh, A. S. Highly Selective Syngas/H₂ Production via Partial Oxidation of CH₄ Using (Ni, Co and Ni-Co)/ZrO₂-Al₂O₃ Catalysts: Influence of Calcination Temperature. *Processes* **2019**, *7*, 141.

(45) Wu, H.; Zou, M.; Guo, L.; Ma, F.; Mo, W.; Yu, Y.; Mian, I.; Liu, J.; Yin, S.; Tsubaki, N. Effects of calcination temperatures on the structure-activity relationship of Ni-La/Al₂O₃ catalysts for syngas methanation. *RSC Adv.* **2020**, *10*, 4166–4174.

(46) Gálvez, M. E.; Albarazi, A.; Da Costa, P. Enhanced catalytic stability through non-conventional synthesis of Ni/SBA-15 for methane dry reforming at low temperatures. *Appl. Catal., A* **2015**, *504*, 143–150.

(47) Wang, Y.; Li, L.; Wang, Y.; Da Costa, P.; Hu, C. Highly Carbon-Resistant Y Doped NiO-ZrO_m Catalysts for Dry Reforming of Methane. *Catalysts* **2019**, *9*, 1055.

(48) Li, C.; Fu, Y.; Bian, G.; Hu, T.; Xie, Y.; Zhan, J. CO₂ reforming of CH₄ over Ni/CeO₂-ZrO₂-Al₂O₃ prepared by hydrothermal synthesis Method. *J. Nat. Gas Chem.* **2003**, *12*, 167–177.

(49) Świrk, K.; Rønning, M.; Motak, M.; Beaunier, P.; Da Costa, P.; Grzybek, T. Ce-and Y-Modified Double-Layered Hydroxides as Catalysts for Dry Reforming of Methane: On the Effect of Yttrium Promotion. *Catalysts* **2019**, *9*, 56.

(50) Li, D.; Nishida, K.; Zhan, Y.; Shishido, T.; Oumi, Y.; Sano, T.; Takehira, K. Sustainable Ru-doped Ni catalyst derived from hydrothermalite in propane reforming. *Appl. Clay Sci.* **2009**, *43*, 49–56.

(51) Świrk, K.; Gálvez, M. E.; Motak, M.; Grzybek, T.; Rønning, M.; Da Costa, P. Dry reforming of methane over Zr-and Y-modified Ni/Mg/Al double-layered hydroxides. *Catal. Commun.* **2018**, *117*, 26–32.

(52) Świrk, K.; Gálvez, M. E.; Motak, M.; Grzybek, T.; Rønning, M.; Da Costa, P. Syngas production from dry methane reforming over yttrium-promoted nickel-KIT-6 catalysts. *Int. J. Hydrogen Energy* **2019**, *44*, 274–286.

(53) Sutthiumporn, K.; Kawi, S. Promotional effect of alkaline earth over Ni-La₂O₃ catalyst for CO₂ reforming of CH₄: Role of surface oxygen species on H₂ production and carbon suppression. *Int. J. Hydrogen Energy* **2011**, *36*, 14435–14446.

(54) Chen, X.; Yik, E.; Butler, J.; Schwank, J. W. Gasification characteristics of carbon species derived from model reforming compound over Ni/Ce-Zr-O catalysts. *Catal. Today* **2014**, *233*, 14–20.

(55) Czekaj, I.; Loviat, F.; Raimondi, F.; Wambach, J.; Biollaz, S.; Wokaun, A. Characterization of surface processes at the Ni-based catalyst during the methanation of biomass-derived synthesis gas: X-ray photoelectron spectroscopy (XPS). *Appl. Catal., A* **2007**, *329*, 68–78.

(56) Imparato, C.; Fantauzzi, M.; Passiu, C.; Rea, I.; Ricca, C.; Aschauer, U.; Sannino, F.; D'Errico, G.; De Stefano, L.; Rossi, A.; Arrone, A. Unraveling the Charge State of Oxygen Vacancies in ZrO_{2-x} on the Basis of Synergistic Computational and Experimental Evidence. *J. Phys. Chem. C* **2019**, *123*, 11581–11590.

(57) Ma, W.; Herbert, F. W.; Senanayake, S. D.; Yildiz, B. Non-equilibrium oxidation states of zirconium during early stages of metal oxidation. *Appl. Phys. Lett.* **2015**, *106*, 101603.

(58) Liu, G.; Rodriguez, J. A.; Hrbek, J.; Dvorak, J.; Peden, C. H. F. Electronic and chemical properties of Ce_{0.8}Zr_{0.2}O₂ (111) surfaces: photoemission, XANES, density-functional, and NO₂ adsorption studies. *J. Phys. Chem. B* **2001**, *105*, 7762–7770.

(59) Liao, W.; Zheng, T.; Wang, P.; Tu, S.; Pan, W. Efficient microwave-assisted photocatalytic degradation of endocrine disruptor

dimethyl phthalate over composite catalyst ZrO_x/ZnO. *J. Environ. Sci.* **2010**, *22*, 1800–1806.

(60) Matsuoka, M.; Isotani, S.; Chubaci, J. F. D.; Miyake, S.; Setsuhara, Y.; Ogata, K.; Kuratani, N. Influence of ion energy and arrival rate on x-ray crystallographic properties of thin ZrO_x films prepared on Si(111) substrate by ion-beam assisted deposition. *J. Appl. Phys.* **2000**, *88*, 3773–3775.

(61) Saw, E. T.; Oemar, U.; Tan, X. R.; Du, Y.; Borgna, A.; Hidajat, K.; Kawi, S. Bimetallic Ni-Cu catalyst supported on CeO₂ for high-temperature water-gas shift reaction: Methane suppression via enhanced CO adsorption. *J. Catal.* **2014**, *314*, 32–46.

(62) Wang, H.; Liu, J.; Zhao, Z.; Wei, Y.; Xu, C. Comparative study of nanometric Co-, Mn- and Fe-based perovskite-type complex oxide catalysts for the simultaneous elimination of soot and NOx from diesel engine exhaust. *Catal. Today* **2012**, *184*, 288–300.

(63) Liang, H.; Hong, Y.; Zhu, C.; Li, S.; Chen, Y.; Liu, Z.; Ye, D. Influence of partial Mn-substitution on surface oxygen species of LaCoO₃ catalysts. *Catal. Today* **2013**, *201*, 98–102.

(64) Li, Y.; Han, X.; Hou, Y.; Guo, Y.; Liu, Y.; Cui, Y. In situ preparation of mesoporous iron titanium catalysts by a CTAB-assisted process for NO reduction with NH₃. *Appl. Catal., A* **2018**, *559*, 146–152.

(65) Chen, D.; Feng, J.; Sun, J.; Cen, C.; Tian, S.; Yang, J.; Xiong, Y. Molybdenum modified Montmorillonite clay as an efficient catalyst for low temperature NH₃-SCR. *J. Chem. Technol. Biotechnol.* **2020**, *1441*.

(66) Li, X.; Li, D.; Tian, H.; Zeng, L.; Zhao, Z. J.; Gong, J. Dry reforming of methane over Ni/La₂O₃ nanorod catalysts with stabilized Ni nanoparticles. *Appl. Catal., B* **2017**, *202*, 683–694.

(67) Miao, J.-Y.; Yang, L.-F.; Cai, J.-X. Acidities of CeO₂ and Ce_{0.5}Zr_{0.5}O₂ solid solutions studied by NH₃-TPD. *Surf. Interface Anal.* **1999**, *28*, 123–125.

(68) Rossetti, I.; Biffi, C.; Bianchi, C. L.; Nichele, V.; Signoreto, M.; Menegazzo, F.; Finocchio, E.; Ramis, G.; De Michele, A. Ni/SiO₂ and Ni/ZrO₂ catalysts for the steam reforming of ethanol. *Appl. Catal., B* **2012**, *117–118*, 384–396.

(69) Sadykov, V. A.; Simonov, M. N.; Mezentseva, N. V.; Pavlova, S. N.; Fedorova, Y. E.; Bobin, A. S.; Bepalko, Y. N.; Ishchenko, A. V.; Krieger, T. A.; Glazneva, T. S.; Larina, T. V.; Cherepanova, S. V.; Kaichev, V. V.; Saraev, A. A.; Chesalov, Y. A.; Shmakov, A. N.; Roger, A.-C.; Adamski, A. Ni-loaded nanocrystalline ceria-zirconia solid solutions prepared via modified Pechini route as stable to coking catalysts of CH₄ dry reforming. *Open Chem.* **2016**, *14*, 363–376.

(70) Chavan, S.; Bonino, F.; Vitillo, J. G.; Groppo, E.; Lamberti, C.; Dietzel, P.; Zecchina, A.; Bordiga, S. Response of CPO-27-Ni towards CO, N₂ and C₂H₄. *Phys. Chem. Chem. Phys.* **2009**, *11*, 9811–9822.

(71) Li, W.; Zhao, Z.; Ding, F.; Guo, X.; Wang, G. Syngas Production via Steam-CO₂ Dual Reforming of Methane over LA-Ni/ZrO₂ Catalyst Prepared by L-Arginine Ligand-Assisted Strategy: Enhanced Activity and Stability. *ACS Sustainable Chem. Eng.* **2015**, *3*, 3461–3476.

(72) Demoulin, O.; Navez, M.; Ruiz, P. Investigation of the behaviour of a Pd/g-Al₂O₃ catalyst during methane combustion reaction using in situ DRIFT spectroscopy. *Appl. Catal., A* **2005**, *295*, 59–70.

(73) Németh, M.; Schay, Z.; Srankó, D.; Károlyi, J.; Sáfrán, G.; Sajó, I.; Horváth, A. Impregnated Ni/ZrO₂ and Pt/ZrO₂ catalysts in dry reforming of methane: Activity tests in excess methane and mechanistic studies with labeled ¹³CO₂. *Appl. Catal., A* **2015**, *504*, 608–620.

(74) Thomas, C. R.; Pihl, J. A.; Lance, M. J.; Toops, T. J.; Parks, J. E., II; Lauterbach, J. Effects of four-mode hydrothermal aging on three-way catalysts for passive selective catalytic reduction to control emissions from lean-burn gasoline engine. *Appl. Catal., B* **2019**, *244*, 284–294.